New Journal of Physics
The open access journal at the forefront of physics

Deutsche Physikalische Gesellschaft DPG
IOP Institute of Physics

Published in partnership with: Deutsche Physikalische Gesellschaft and the Institute of Physics

OPEN ACCESS

RECEIVED
17 December 2015

REVISED
31 March 2016

ACCEPTED FOR PUBLICATION
11 May 2016

PUBLISHED
26 May 2016

PAPER

Observation of spatially oscillating solitons in photonic lattices

F Diebel, P Rose, M Boguslawski and C Denz

Institut für Angewandte Physik and Center for Nonlinear Science (CeNoS), Westfälische Wilhelms-Universität Münster, D-48149 Münster, Germany

E-mail: falko.diebel@uni-muenster.de

Keywords: optical solitons, nonlinear optics, nondiffracting beams, photonic lattices, photorefractive nonlinearity

Abstract

We report on the experimental observation of spatially oscillating solitons in two-dimensional nonlinear photonic lattices, realized by optical induction using a continuous nondiffracting Weber beam. Thereby, we introduce and demonstrate a new type of transverse soliton dynamics originating from the unique parabolic geometry of the photonic lattice. First, we numerically calculate the fundamental soliton solution for this lattice and experimentally demonstrate its existence. Afterwards, we experimentally launch the soliton with an additional transverse momentum and observe harmonic spatial oscillation during propagation.

1. Introduction

Solitons as one of the most fundamental solution in nonlinear systems have been found in rather different fields of science such as atomic physics [1, 2], molecular biology [3], and optics [4–6] where they have been subject of extensive theoretical and experimental research within the last decades. The first observation of a solitary water wave by Russel in 1834 [7] can be regarded as the birth of the research on solitons. Solitons describe nonlinearly localized wave packets that do not change their shape during propagation and can be divided into two classes—spatial or temporal—depending on whether the wave packet is localized in space or time, moreover also spatio-temporal solitons exist [8, 9].

Spatial solitons are of particular interest, basically because their fundamental physics is richer compared to that of temporal solitons and nonlinear confinement can occur in both, one and two transverse dimensions. If the conditions for a spatial soliton are fulfilled, the broadening of the localized excitation caused by ubiquitous diffraction is exactly balanced by nonlinear localization. Consequently, the solution propagates as a form-stable wave packet, which additionally exhibits particle-like interactions. One appropriate type of nonlinear response which enables stable two-dimensional spatial solitons is known as the photorefractive effect [10, 11]. In 1992, the demonstration of photorefractive solitons [12] as a new type of spatial solitons launched an inventive field of research on nonlinear light propagation.

To increase the diversity of soliton dynamics, their nonlinear evolution can be studied inside photonic lattices [5, 13, 14]. The complex interplay between nonlinearity and optically induced refractive index landscapes facilitates a multitude of novel approaches to control light by light itself for all-optical data processing and routing [15–18]. A comprehensive overview of solitons in various photonic lattices can be found in [19]. Beyond well studied classical solitons, we introduce and observe a new type of spatially oscillating solitons featured by a specifically shaped photonic potential. In contrast to breather solitons [6], where the oscillation appears in the amplitude, the focus now is set to spatial oscillation with constant amplitude. As earlier numerical studies in an idealized model system have revealed, in fact, the refractive index lattice can be designed to feature such fascinating types of soliton dynamics [20]. Moreover, spatially oscillating solitons could be observed in different nonlinear systems such as Fermi gases [21] and Bose–Einstein condensates [22, 23].

In this contribution, we report on experimental observation of stable oscillating solitons in two-dimensional photonic lattices. We demonstrate a new type of complex transverse soliton dynamics that is enabled by the unique parabolic geometry of the photonic lattice that is optically induced by a continuous nondiffracting Weber beam [24]. First, we numerically calculate the fundamental stationary soliton for the Weber lattice and

experimentally verify stable propagation of this so-called fundamental Weber soliton. Thereby, we perform a paradigm change in optical soliton experiments by directly using numerical results as input probe beams rather than probing the system with a Gaussian beam and waiting for the soliton to be formed. With the existence of the fundamental Weber soliton be proven, we launch this Weber soliton with an additional transverse momentum. This causes a spatial oscillation of the Weber soliton that propagates stably through the parabolic curved two-dimensional photonic lattice and in this way represents a new interesting type of soliton dynamics.

2. Two-dimensional nondiffracting Weber beam

Since we consider light propagation in two-dimensional photonic lattices, our approach of optical induction requires intensity distributions for the inscription that are modulated in the transverse dimensions but remain invariant in direction of propagation. Such field distributions are referred to as nondiffracting beams [24]. For monochromatic light fields with harmonic time dependence, the general solution of the Helmholtz equation for a given transverse wave vector component $k_\perp$ can be expressed in terms of a reduced Whittaker integral [25]

$$\psi(\mathbf{r},\, t) = \mathrm{e}^{-\mathrm{i}\omega t}\mathrm{e}^{\mathrm{i}k_z z}\int_{-\pi}^{\pi} \mathrm{e}^{\mathrm{i}k_\perp (x\cos\varphi + y\sin\varphi)} f(\varphi)\,\mathrm{d}\varphi, \tag{1}$$

where $f(\varphi)$ is an arbitrary complex function, $k^2 = k_\perp^2 + k_z^2$ denotes the square of the wave number and $\omega = ck$ the angular frequency, with c being the speed of light in medium. The resulting lattice-beam intensity $I_{\mathrm{latt}} = |\psi(\mathbf{r},\, t)|^2$ no longer depends on the propagation distance z, and all transverse spatial frequency components of nondiffracting beams lie on a small ring with radius $k_\perp$ in Fourier space. The rich variety of nondiffracting beams is caused by the complex function $f(\varphi)$ that completely determines the transverse profile [24, 27–28].

In particular, we use a nondiffracting continuous Weber beam to fabricate the two-dimensional photonic lattice by optical induction. This beams shows the specific topology according to the underlying parabolic coordinate system and exhibits an intensity distribution where the separated regions of high intensity follow parabolas and are continuously modulated along them. Near the angular point this modulation is well approximated by a quadratic function. Since the optical induction process will transfer this intensity pattern into a refractive index modulation, although with small deviations, this written index modulation shows the same general features as the writing beam intensity. The angular spectrum of the continuous Weber beam can be expressed as

$$f(\varphi) = (\pi|\sin\varphi|)^{-1/2}\exp(\mathrm{i}a\,\ln|\tan\varphi/2|) \quad \text{for } \varphi \in (0,\,\pi) \tag{2}$$

$$f(\varphi) = 0 \quad \text{for } \varphi \in [-\pi,\,0], \tag{3}$$

where $a = 1.6$ denotes the chosen separation constant [24].

Figures 1(a) and (b) show the intensity distribution of the experimentally realized nondiffracting Weber beam at the front and back face of the used nonlinear crystal. The structure size of the beam is set to $\pi/k_\perp = g \approx 30\ \mu$m, which results in a set of parabolas that are separated by approximately 32 μm. To verify that the writing beam is two-dimensional, we experimentally scan the whole area of the SBN crystal and record the three-dimensional intensity volume. A cross section through this volume along the x-direction (see lines in figures 1(a) and (b)) is shown in figure 1(d). The corresponding numerical simulation of the induced refractive index pattern in figure 1(c) clearly shows the described features of curved parabolas with quadratically modulated strength in the vicinity of the angular point. As one considers the induced refractive index modulation as an attractive potential for the soliton dynamics, besides a stable fundamental soliton, a harmonically oscillating solitary solution is expected for sufficient small oscillation amplitudes [29].

3. Experimental setup and numerical simulation

As nonlinear medium, we use a $5 \times 5 \times 20\ \mathrm{mm}^3$ cerium-doped photorefractive strontium barium niobate (SBN:60) crystal with an external electric field of $E_{\mathrm{ext}} = 1.6\ \mathrm{kV\ cm}^{-1}$ applied along the crystalline c-axis to gain self-focusing nonlinearity. The nonlinearity is caused by an incident spatially modulated light intensity that locally excites charge carriers via photoionization which are redistributed by drift in the external electric field. The resulting internal space charge field modulates the refractive index via the linear electro-optic effect [30]. This way, we can generate arbitrary pre-designed refractive index modulations in a highly reconfigurable way, while at the same time getting high nonlinearity at low power levels, as successfully demonstrated in many applications [5, 28, 31]. Moreover, the strong polarization anisotropy in the electro-optic coefficients of SBN ($r_{33} \gg r_{13}$) allows us to realize a nonlinear environment for the extraordinary polarized probe beam, while the ordinarily polarized lattice beam experiences only negligible nonlinearity.

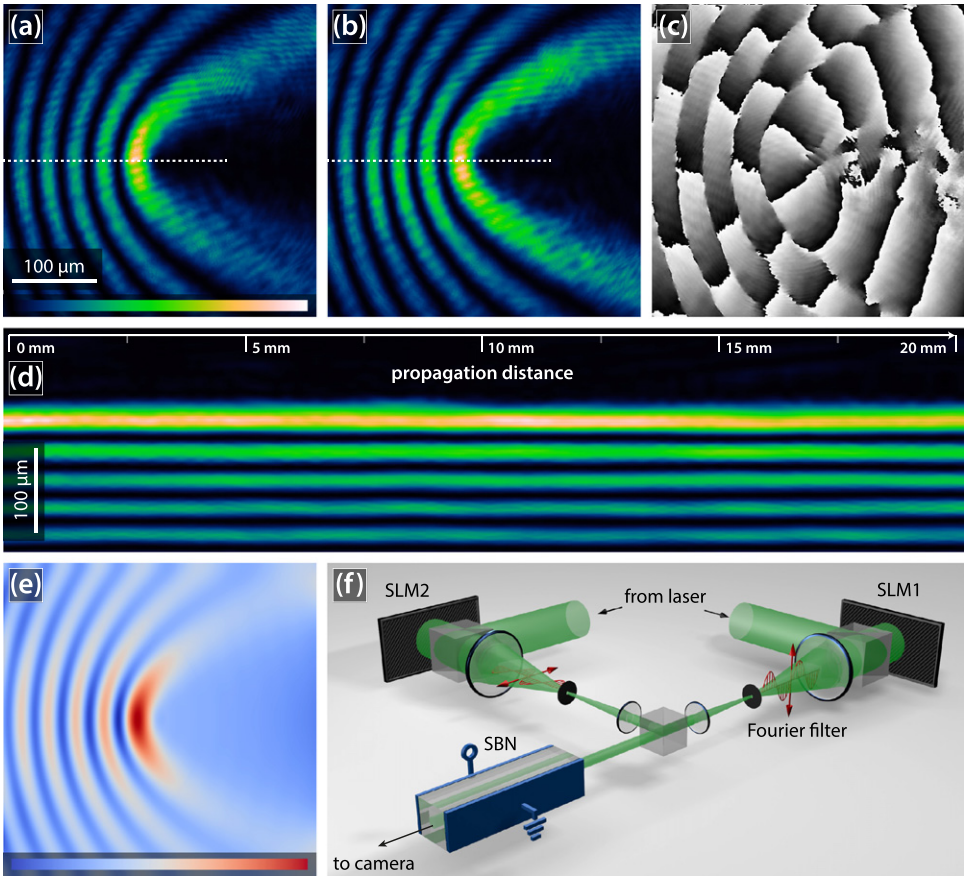

Figure 1. Characteristics of the nondiffracting Weber beam and the experimental setup. (a) and (b) Experimentally recorded intensity distributions at the input and output face of the crystal. (c) Measured phase profile at the output face. (d) Cross-section through the experimentally recorded three-dimensional intensity volume along the line shown in (a) and (b). (e) Numerically calculated induced refractive index modulation. (f) Experimental setup.

All experiments were performed using the setup sketched in figure 1(f). Light from a frequency-doubled Nd:YVO_4 laser emitting continuously at $\lambda_0 = 532$ nm is divided into two beams, each illuminating a high-resolution programmable phase-only spatial light modulator. The first modulator (SLM 1) shapes the lattice beam by impressing a pre-calculated phase distribution onto the wave field, wherein both, phase and amplitude information of the complex nondiffracting beam are encoded [32]. Using a 4f-system, including a spatial low-pass filter in Fourier plane, the lattice wave is imaged onto the front face of the nonlinear medium. In a similar way, the second beam—referred to as probe beam—is generated by the second modulator (SLM 2) and also imaged onto the front face, where both beams are exactly overlain. A camera mounted on a translation stage records the field distribution at different positions along the propagation direction. With this setup we are able to realize all types of (nondiffracting) beams for optical induction, as well as any desired field distribution as a probe beam and investigate its nonlinear dynamics in the experiment.

To numerically simulate the nonlinear light propagation of the probe beam A, we implemented a spectral split-step beam propagation method to solve the scaled nonlinear Schrödinger equation for the slowly varying field envelope:

$$\partial_z A(\mathbf{r}) = \left[\frac{\mathrm{i}}{2}\nabla_\perp^2 - \frac{\mathrm{i}}{2}\gamma_{\mathrm{nl}} E_{\mathrm{sc}}(I_{\mathrm{tot}})\right] A(\mathbf{r}), \tag{4}$$

with $\gamma_{\mathrm{nl}} = k_0^2 w_0^2 n_0^4 r_{\mathrm{eff}}$, a transverse scaling w_0, $n_0 = 2.325$, $r_{\mathrm{eff}} = 237$ pm V^{-1}, and $I_{\mathrm{tot}} = I_{\mathrm{lattice}} + |A|^2$ [33]. The induced space-charge field $E_{\mathrm{sc}} = -\nabla_\perp \phi_{\mathrm{sc}}$ is given by the reduced potential equation of the full anisotropic model [34]:

$$\nabla_\perp^2 \phi_{\mathrm{sc}} + \nabla_\perp \ln(1+\tilde{I})\nabla_\perp \phi_{\mathrm{sc}} = E_{\mathrm{ext}} \frac{\partial}{\partial x} \ln(1+\tilde{I}) + \frac{k_B T}{e}[\nabla_\perp^2 \ln(1+\tilde{I}) + (\nabla_\perp \ln(1+\tilde{I}))^2], \tag{5}$$

where $\tilde{I} \propto I_{\mathrm{tot}}$ is the intensity scaled by the dark conductivity of the SBN crystal. The solutions of this equation are calculated using relaxation methods. Finally, the transverse profile $a(\mathbf{r}_\perp)$ of the solitary solution in the form

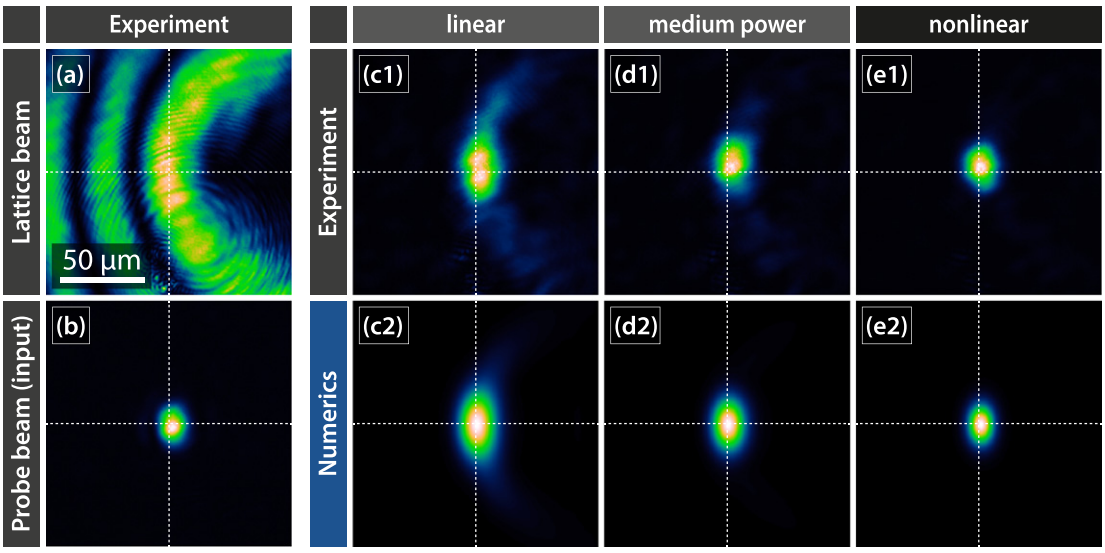

Figure 2. Experimental observation of a fundamental Weber soliton. (a) Lattice wave intensity at the crystal back face, (b) probe beam intensity at the input face. (c) Wave guiding in linear regime, (d) confined state at moderate power, (e) stable Weber soliton at correct power ($P_{\mathrm{probe}} \approx 17$ nW). (Top row) Experiments, (bottom row) numerical simulations. All panels are individually normalized.

$A(\mathbf{r}) = a(\mathbf{r}_\perp)\exp(\mathrm{i}\beta z)$, with β being the propagation constant of the soliton, is calculated employing a modified Petviashvili iteration scheme [35].

4. Fundamental Weber soliton

As the first step, we want to experimentally demonstrate the existence of a stable fundamental Weber soliton inside the photonic Weber lattice. This potential is optically induced by a continuous Weber beam with a total power of $P_{\mathrm{lattice}} = 1.9\ \mu$W. To see the build-up process of the fundamental Weber soliton, we perform the transition from linear wave guiding to nonlinear light localization by successively increasing the probe beam power. The initial field distribution at the input, shown in figure 2(b), is given by the numerically calculated soliton profile that is directly transferred to the experiment. The experimentally recorded intensity distributions at the back face of the crystal are shown in figures 2(c)–(e) (top row) and compared with the numerical simulations (bottom row).

In the linear regime (see figure 2(c)), the soliton launched at the front face of the crystal diffracts and is only guided linearly by the induced refractive index structure. Consequently, the intensity distribution is well localized in horizontal direction, but broadened along the parabola. In contrast, for the correct input power of $P_{\mathrm{probe}} \approx 17$ nW, the nonlinearity is exactly adjusted as requested to form the fundamental Weber soliton (see figure 2(e)). The intensity now is well confined in both transverse directions and the resulting output profile is almost identical to the input while remaining temporally constant. Thus we clearly can identify this field distribution as a stable photorefractive Weber soliton that propagates stably through the crystal, what corresponding numerical simulations additionally confirm.

5. Spatially oscillating Weber soliton

Now, we want to explore the spatial dynamics and oscillation of this Weber soliton. To enable oscillation, we impose a linear phase gradient onto the field distribution of the fundamental soliton in order to introduce a transverse momentum which is required to have spatial dynamics and oscillation. The transverse momentum is adapted to the tangent of the parabola in which the corresponding soliton is launched.

Our numerical simulations indeed reveal an oscillatory trajectory of the Weber soliton launched with an initial transverse momentum, while it stably propagates through the nonlinear photorefractive crystal. Figure 3(a) displays the intensity distribution of the soliton simulated for a propagation length that exactly covers two periods. This result nicely confirms that the transverse displacement of the soliton follows an oscillating trajectory while it stays localized and almost unchanged.

By calculating the transverse center of mass of the soliton intensity profile as $s_\chi(z) = \int \chi\, I(\mathbf{r})\mathrm{d}\mathbf{r}_\perp \big/ \int I(\mathbf{r})\mathrm{d}\mathbf{r}_\perp$, $\chi = \{x, y\}$ (figure 3(b)) we can see that the oscillation predominantly occurs

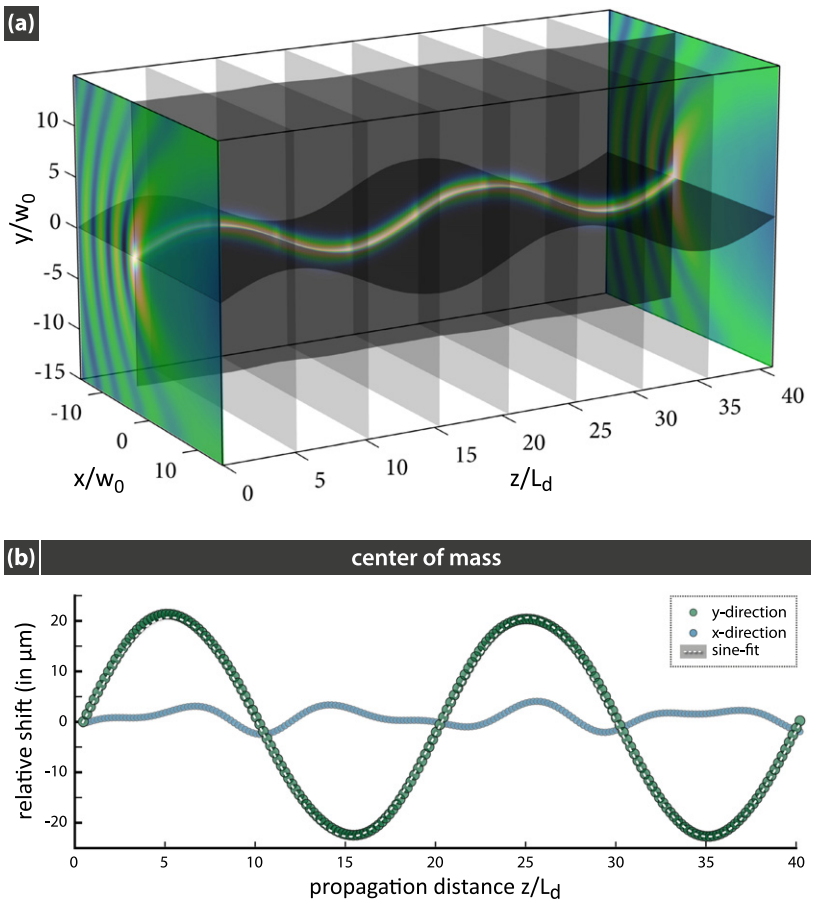

Figure 3. Oscillating Weber soliton. Numerically simulated propagation of the fundamental soliton launched at $z = 0$ with an initial transverse momentum. (a) The three-dimensional intensity distribution of the propagating soliton inside the crystal with two oscillation periods being captured. The transverse x, y and longitudinal coordinates z are scaled by characteristic lengths w_0 and $L_d = kw_0^2$, respectively. (b) Calculated center of mass (x and y component). The y component is fitted with a sine curve.

in y-direction with an amplitude of 22 μm, while the displacement in x-direction is always less than 4 μm. Moreover, by fitting the y-component with a sine curve the oscillation turns out to be harmonic with a dimensionless period of $\Lambda_z' \approx 20.6$, what corresponds to physical length of $\Lambda_z \approx 57$ mm. Consequently, the maximal propagation angle of the soliton with respect to the z axis is $\alpha_{\max} \approx 0.14°$, as the maximum slope of the center of mass curve $\alpha_{\max} = \max[\partial_z s_y(z)]$.

If the transverse momentum of the soliton is increased, the soliton starts to enter regions of the transverse index modulation, where the potential no longer is quadratic along the trajectory of the soliton. Following, the soliton becomes anharmonic and unstable. If the transverse momentum is further increased, the depth of the potential will not be sufficient to trap the soliton and finally it will travel simply across the lattice. We observed this behavior in numerical simulations.

With the numerical results at hand, we finally want to demonstrate the oscillating Weber soliton also in the experiment. Here, we are faced with a principle problem. Since the oscillation happens during propagation through the nonlinear crystal, it would be necessary to look inside the volume in order to track the trajectory. But it is not possible to directly analyze the field distribution inside an inhomogeneous medium with an in general unknown refractive index modulation imprinted. We bypass this experimental limitation and verify the oscillation indirectly by taking advance of the remarkable interplay between the experimental situation and our implemented numerical simulation.

As the soliton oscillates with respect to the propagation distance z, we effectively change the length of the crystal by numerically propagating the initial field distribution of the oscillating Weber soliton for different distances Δz_{num} before mapping the numerical results accurately onto the input face of the SBN crystal in the experiment. Thus, the total effective length L_{eff} is the sum of the fixed length of the SBN crystal (L_{SBN}) and the variable numerical distance (Δz_{num}).

Figure 4 illustrates the idea behind this method. We extract nine different equidistant slices from the numerically simulated data that cover one full oscillation period. These different field distributions serve as input states for the experiment and will propagate through the SBN crystal. According to the multiple input

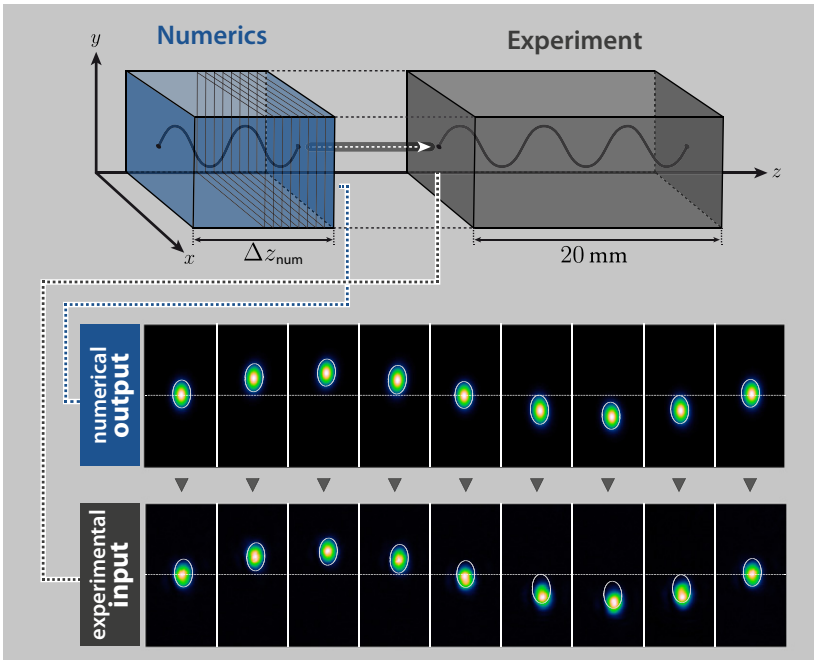

Figure 4. Illustration of the basic idea behind the method to verify the oscillation. The effective propagation length for the soliton is the sum of a numerical distance Δz_{num} and the fixed length of the SBN crystal L_{SBN}. After numerical propagation, the respective solution (numerical output) is directly transferred to the experiment (experimental input).

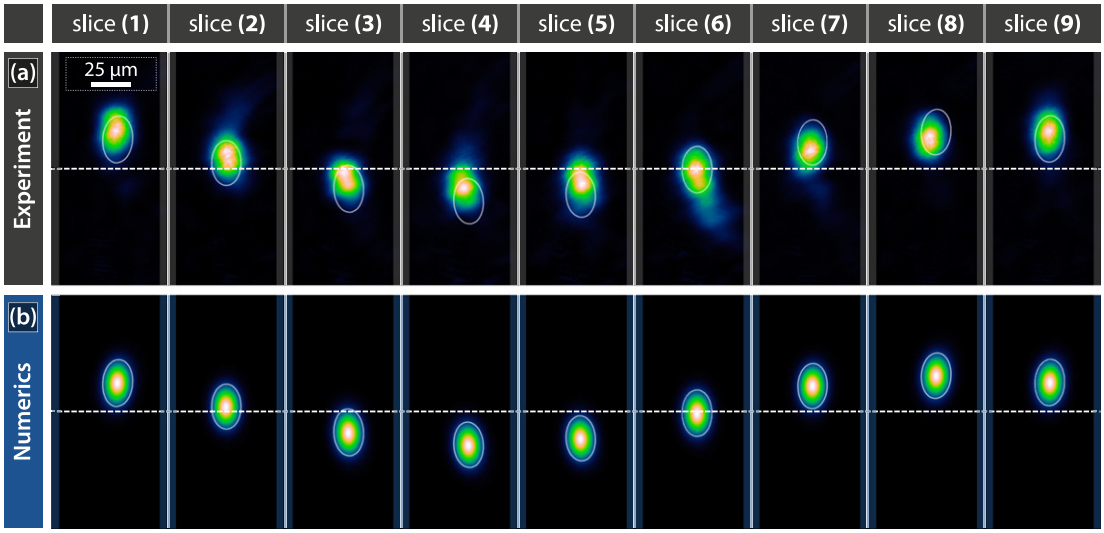

Figure 5. Experimental observation of the oscillating Weber soliton. (a) Recorded intensity distributions of the oscillating Weber soliton at the back face of the SBN crystal for nine different initial conditions. (b) Results of the corresponding numerical simulations. The white contour line indicates the $1/e^2$-value of the maximum intensity of the numerically simulated soliton.

states, the field distribution at the output should also be different and correspond to $L_{\text{eff}} = L_{\text{SBN}} + \Delta z_{\text{num}} = L_{\text{SBN}} + m\,\frac{\Lambda_z}{8}$, $m = 0 \ldots 8$. Thus, they also should span over one period, but a shifted part of the oscillation. With this approach it is possible to experimentally verify the oscillation of the soliton, although it is impossible to look inside the inhomogeneous medium.

The experimental results for the oscillating Weber soliton are shown in figure 5. It shows the experimentally recorded output profiles for the soliton that has propagated through the crystal. Following our method to verify the oscillation, we launch the soliton for nine different oscillation states that correspond to different numerical propagation lengths, see figure 5. According to the particular input profiles, the soliton recorded at the output (figure 5(a)) appears at the corresponding transverse positions that are expected after propagation through the

medium. For comparison, we show the numerically simulated output profiles (bottom row). The iso-value lines plotted therein (at $1/e^2$ of the maximal intensity) are transferred to the experimental data.

The varying transverse displacement of the soliton at the output clearly describes a whole period of a harmonic spatial oscillation. This, together with its nonlinear spatial localization along the induced refractive index parabola, strongly indicates the new type of spatial soliton oscillation in a photonic Weber lattice. In addition, there is an excellent agreement between these experimental results in figure 5(a) and the corresponding numerical simulations in figure 5(b). All together, this confirms the experimental observation of oscillating Weber solitons in photorefractive photonic lattices and substantiates our original approach to combine numerical simulations with the actual experiment.

6. Conclusions

In conclusion, we have successfully demonstrated the experimental observation of oscillating spatial solitons in curved photonic lattices. This new type of soliton dynamics is facilitated by the unique properties of the optically induced photonic Weber lattice, exhibiting refractive index parabolas with quadratically modulated strength alongside. Our findings were corroborated and enabled by accurate numerical simulations of the nonlinear light propagation in the anisotropic photorefractive material.

In a first step, we have proven the existence of a fundamental soliton in the Weber lattice, before exploring its spatial dynamics and oscillation. Due to the comprehensive agreement between the experiment and the numerics we are able to vary the effective length of the nonlinear crystal in order to resolve the z-dependent spatial oscillation of the Weber soliton. The presented results and the introduced original experimental methods will pave the way towards further studies on spatial solitons and their propagation dynamics in various physical contexts.

Acknowledgments

We acknowledge support by Open Access Publication Fund of University of Muenster.

References

[1] Burger S, Bongs K, Dettmer S, Ertmer W, Sengstock K, Sanpera A, Shlyapnikov G V and Lewenstein M 1999 *Phys. Rev. Lett.* **83** 5198–201
[2] Denschlag J, Simsarian J and Feder D 2000 *Science* **287** 97
[3] Davydov A S and Kislukha N I 1973 *Phys. Status Solidi* **59** 465
[4] Chiao R, Garmire E and Townes C 1964 *Phys. Rev. Lett.* **13** 479
[5] Fleischer J W, Segev M, Efremidis N K N and Christodoulides D N 2003 *Nature* **422** 147
[6] Kivshar Y S and Agrawal G P 2003 *Optical Solitons: From Fibers to Photonic Crystals* (San Diego: Academic)
[7] Russell J S 1845 *Report of the 14th Meeting of the British Association for the Advancement of Science* (*York*) vol 1844 pp 311
[8] Malomed B A, Mihalache D, Wise F and Torner L 2005 *J. Opt. B: Quantum Semiclass. Opt.* **7** R53
[9] Minardi S *et al* 2010 *Phys. Rev. Lett.* **105** 263901
[10] Ashkin a, Boyd G D, Dziedzic J M, Smith R G, Ballman a a, Levinstein J J and Nassau K 1966 *Appl. Phys. Lett.* **9** 72
[11] Chen F S 1968 *Appl. Phys. Lett.* **13** 223
[12] Segev M, Crosignani B, Yariv A and Fischer B 1992 *Phys. Rev. Lett.* **68** 923
[13] Christodoulides D N, Lederer F and Silberberg Y 2003 *Nature* **424** 817
[14] Terhalle B *et al* 2009 *Phys. Rev.* A **79** 043821
[15] Mingaleev S and Kivshar Y S 2002 *Opt. Photonics News* **13** 48
[16] Keil R, Heinrich M, Dreisow F, Pertsch T, Tünnermann A, Nolte S, Christodoulides D N and Szameit A 2011 *Sci. Rep.* **1** 94
[17] Rose P, Diebel F, Boguslawski M and Denz C 2013 *Appl. Phys. Lett.* **102** 101101
[18] Diebel F, Leykam D, Boguslawski M, Rose P, Denz C and Desyatnikov A S 2014 *Appl. Phys. Lett.* **104** 261111
[19] Kartashov Y V, Vysloukh V A and Torner L 2009 *Prog. Opt.* **52** 63
[20] Ruelas A, Lopez-Aguayo S and Gutiérrez-Vega J C 2008 *Opt. Lett.* **33** 2785
[21] Scott R G, Dalfovo F, Pitaevskii L P and Stringari S 2011 *Phys. Rev. Lett.* **106** 185301
[22] Bongs K, Burger S, Birkl G, Sengstock K, Ertmer W, Rzazewski K, Sanpera A and Lewenstein M 1999 *Phys. Rev. Lett.* **83** 3577
[23] Becker C, Stellmer S, Soltan-Panahi P, Dörscher S, Baumert M, Richter E M, Kronjäger J, Bongs K and Sengstock K 2008 *Nat. Phys.* **4** 496
[24] Durnin J, Miceli J J J and Eberly J H 1987 *Phys. Rev. Lett.* **58** 1499
[25] Whittaker E T 1927 *A Course of Modern Analysis* 4th edn (Cambridge: Cambridge University Press)
[26] Bouchal Z Z 2003 *Czech. J. Phys.* **53** 537
[27] Rose P, Boguslawski M and Denz C 2012 *New J. Phys.* **14** 033018
[28] Bandres M A, Gutiérrez-Vega J C and Chávez-Cerda S 2004 *Opt. Lett.* **29** 44
[29] Kartashov Y V, Vysloukh V A and Torner L 2008 *Opt. Lett.* **33** 141
[30] Kukhtarev N V, Markov V B, Odulov S G, Soskin M S and Vinetskii V L 1978 *Ferroelectrics* **22** 949
[31] Desyatnikov A S, Sagemerten N, Fischer R, Terhalle B, Träger D, Neshev D N, Dreischuh A, Denz C, Królikowski W and Kivshar Y S 2006 *Opt. Express* **14** 2851
[32] Davis J A, Cottrell D M, Campos J, Yzuel M J and Moreno I 1999 *Appl. Opt.* **38** 5004

[33] Stepken A 2001 *Optische Räumliche Solitonen in Photorefraktiven Kristallen* (Aachen: Shaker Verlag)
[34] Zozulya A A and Anderson D Z 1995 *Phys. Rev.* A **51** 1520
[35] Lakoba T I and Yang J 2007 *J. Comput. Phys.* **226** 1668